The real part of the permittivity obtained by the standard offset short calibration is shown as a dashed line in Fig. 2, while the result obtained by the proposed procedure is shown as a continuous line. The plot shows the failure of the standard offset short calibration around 12.6 GHz. To show the stability of the calibration in relation to uncertainty in the position of the sliding short, an error uniformly distributed in ± 0.05 mm has been considered. The maximum and minimum value obtained by applying the proposed calibration are shown in Fig. 2 for some frequencies as error bars. The Figure also shows the maximum and minimum value obtained by the standard offset short calibration, limited by vertical arrows. The error bars are always shorter than the vertical arrows, indicating better stability of the proposed technique compared to the standard procedure. Similar results have been obtained for the imaginary part of the permittivity, confirming the effectiveness of the proposed procedure.

21 January 2003
Electronics Letters Online No: 20030343
DOI: 10.1049/el:20030343

M.D. Migliore (*DAEIMI, Università degli Studi di Cassino, Via Di Biasio 43, 03043 Cassino (FR), Italy*)

E-mail: md.migliore@unicas.it

References

1 BRYANT, G.H.: 'Principles of microwave measurements' (Peter Peregrinus Ltd., London, 1988)
2 SCALZI, G.J., SLOBODNIK, A.J., and ROBERTS, G.A.: 'Network analyzer calibration using offset short', *IEEE Trans. Microw. Theory Techn.*, 1988, **36**, (6), pp. 1097–1100
3 OPPENHEIM, A.V., and SCHAFFER, R.W.: 'Digital signal processing' (Prentice-Hall, Inc., Englewood Cliffs, NJ, 1975)
4 GOLUB, G.H, and VAN LOAD, C.F.: 'Matrix computations' (Johns Hopkins University Press, 1989)
5 SUCHER, M., and FOX, J.: 'Handbook of microwave measurements' (John Wiley & Sons, New York, 1963), Vol. II

Temperature dependence of attenuation of coplanar waveguide on semi-insulating 4H-SiC through 540°C

G.E. Ponchak, Z.D. Schwartz, S.A. Alterovitz, A.N. Downey and J.C. Freeman

For the first time, the temperature and frequency dependence of the attenuation of a coplanar waveguide on semi-insulating 4H-SiC substrate is reported. At 500°C, the attenuation increases by 2 dB/cm at 1 GHz and by 3.25 dB/cm at 50 GHz. This appears to be mainly due to a decrease in the SiC resistivity as the temperature increases.

Introduction: There is a need for sensors with wireless communication capabilities that operate at high temperature (>500°C) for aircraft engine development and its monitoring during flight. Because of the high temperature, wide-bandgap semiconductors such as SiC are required. SiC resistivity has been characterised against temperature using a four-point probe [1], but this only yields the DC material characteristics of the SiC. To fabricate a wireless communication circuit, the RF characteristics of microwave transmission lines against frequency and temperature are required. In this Letter, for the first time the attenuation of a coplanar waveguide (CPW) fabricated on a 4H-SiC is reported over a frequency band of 1 to 50 GHz and a temperature range of 29°C (room temperature) to 540°C.

Circuit description: The substrate is a 4H-SiC wafer with a thickness of 409 μm and a room temperature resistivity greater than $10^5\ \Omega$ cm [2]. An RCA clean was performed on the wafer prior to processing. A set of CPW lines with a centre conductor width, slot width, and ground plane width of 50, 25, and 150 μm, respectively, were fabricated on the wafer using liftoff processing. No insulator was grown over the SiC prior to metal deposition, which consisted of 20 nm of Ti and 1.5 μm of evaporated Au. The set of CPW lines had lengths of 5000, 5850, 6700, 8500, and 17 500 μm.

Measurement procedure: 1 to 50 GHz measurements were made with an HP8510C vector network analyser, an RF probe station, and GGB Industries picoprobes specially built for high temperature probing. Thermal shields were built onto the probes and coaxial cables to reduce the heating of these parts. The conventional probe station wafer chuck was replaced with a specially built wafer chuck consisting of a NASA shuttle tile. Upon the shuttle tile, a computer controlled ceramic heater was placed. The SiC sample was placed on an Si wafer that rested on the ceramic heater. Two thermocouples measured the temperature of the SiC and the Si wafers during measurements and they agreed to within 10°C. At room temperature, a full TRL calibration was performed using all of the CPW lines described above and NIST MULTICAL software [3]. Measurements of the 17 500 μm CPW line were then made from room temperature to 540°C in increments of 30°C.

Results: During measurements, especially above 470°C, the SiC wafer and heater stage glowed red, but the Ti/Au CPW lines showed no visible signs of degradation. However, because the wafer probes were placed down on the CPW probe pads 21 times at high temperature, the probe pads did have visually noticeable wear that caused minor scatter in the measured characteristics.

The room temperature attenuation of the CPW line had the typical frequency dependence that includes a constant term to account for the DC metal resistivity and the portion of the dielectric loss caused by the non-infinite resistivity (ρ) of the SiC substrate, a linear dependence with frequency term to account for the $\tan\delta = \varepsilon''/\varepsilon'$, and an $f^{0.5}$ term to account for conductor loss. The measured attenuation at room temperature is described by:

$$\alpha(RT) = 0.202 + 6.973{*}10^{-3}f + 0.2233f^{0.5} \quad (1)$$

where f is in GHz and $\alpha(RT)$ is in dB/cm. At 50 GHz, the room temperature attenuation is 2.2 dB/cm at 50 GHz. The increase in attenuation above the room temperature attenuation against temperature for 1, 25, and 50 GHz is shown in Fig. 1. It is seen that the attenuation increases by 2 dB/cm at 1 GHz when the temperature is raised to 500°C, while it is increasing by 3.25 dB/cm at 500°C for a frequency of 50 GHz. The increase in attenuation for 25 and 50 GHz is approximately the same.

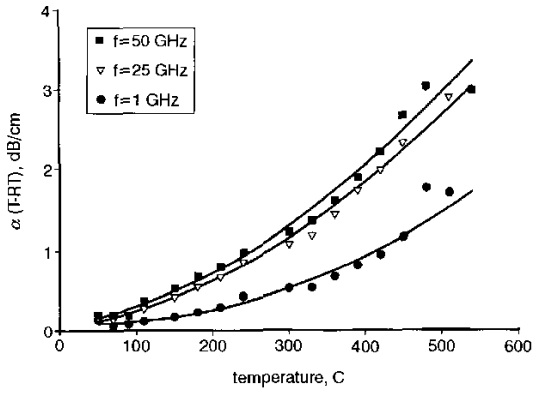

Fig. 1 *Measured increase in attenuation of CPW line against temperature at 1, 25, 50 GHz*

The attenuation of the CPW line was fit to an equation of the same form as (1) at every temperature to determine the nature of the attenuation increase. It is found that the linear term of $\alpha(T-RT)$ is zero, indicating no increase in $\varepsilon''/\varepsilon'$ with temperature and resulting in an additional attenuation given by:

$$\alpha(T - RT) = y_0(T) + b(T)f^{0.5} \quad (2)$$

The constant and the $f^{0.5}$ term dependence on temperature are shown in Fig. 2. The constant term is seen to increase significantly against temperature, while the $f^{0.5}$ term increases nearly linearly with frequency. For plotting purposes, we approximate the temperature dependence of $b(T)$ as T^2.

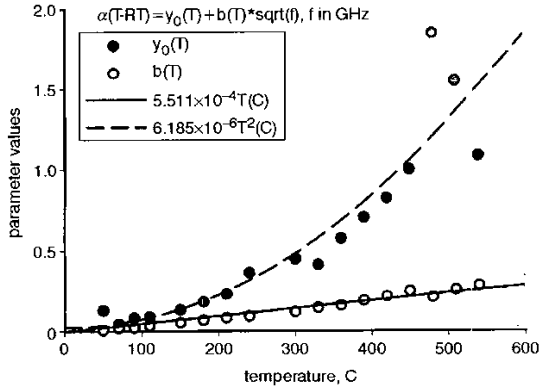

Fig. 2 *Extracted parameter values y_0 and b of (2) for the frequency dependent increase in attenuation of CPW lines against temperature*

These results indicate that SiC wireless circuits may be made on SiC wafers for operation at high temperatures, but at 500°C, the attenuation of microwave transmission lines will increase by approximately 3.25 dB/cm at 50 GHz and 2 dB/cm at 1 GHz. Although further analysis is required, we reason that the major cause for this increase in transmission line attenuation appears to be due to a decrease in the SiC resistivity [1].

Acknowledgment: This work was sponsored by the Ultra-Efficient Engine Technology Program at NASA Glenn Research Center.

12 February 2003
Electronics Letters Online No: 20030356
DOI: 10.1049/el:20030356

G.E. Ponchak, S.A. Alterovitz, A.N. Downey and J.C. Freeman (*NASA Glenn Research Center, 21000 Brookpark Rd., MS 54/5, Cleveland, OH 44135, USA*)

E-mail: george.ponchak@ieee.org

Z.D. Schwartz (*Analex Corp. at NASA Glenn Research Center, 21000 Brookpark Rd., MS 54/5, Cleveland, OH 44135*)

References

1 CLARKE, R.C., BRANDT, C.D., SRIRAM, S., SIERGIEJ, R.R., MORSE, A.W., AGARWAL, A.K., CHEN, L.S., BALAKRISHNA, V., and BURK, A.A.: 'Recent advances in high temperature, high frequency SiC devices'. Proc. 1998 High-Temperature Electronic Materials, Devices, and Sensors Conf., San Diego, CA, USA, 22–27 February 1998, pp. 18–28
2 Cree wafer number BV0302-11, part number W4TRD8R-0D00
3 MARKS, R.B.: 'A multiline method of network analyzer calibration', *IEEE Trans. Microw. Theory Tech.*, 1991, **39**, pp. 1205–1215

Wideband RF photonic vector sum phase-shifter

L.A. Bui, A. Mitchell, K. Ghorbani and T.-H. Chio

A novel broadband linear phase phase-shifter based on the vector summation method is proposed. A photonic implementation of the phase-shifter with a continuously variable linear phase-shift up to 120° over the frequency range of DC–4 GHz is demonstrated. Good agreement between the measured responses and theoretical predictions is obtained.

Introduction: In many advanced defence and radio astronomy applications there is an increasing demand for instantaneous wideband phased array systems. The steering of such phased array systems is often achieved using true-time delay (TTD) units for the broadband beam squint-free operation.

There are many papers describing photonic implementations of TTD devices, e.g. [1, 2]; however their application in practical systems is limited due to their complexity and cost.

A variable feedback photonic phase-shifter (VFPPS) was developed recently and showed that it is possible to achieve phase-shifts that are approximately linear with respect to frequency [3]. The VFPPS operates by coupling light into a resonant feedback loop. The VFPPS that exhibited variable phase-shifts through the application of a biasing voltage was demonstrated from DC to 1.2 GHz [3].

For the device to operate at higher frequencies, the size of the optical feedback loop must be reduced to less than half a wavelength at the highest RF operating frequency. In turn, this puts tremendous pressure on the tolerance and yield of the fabrication process.

In this Letter, we overcome the inherent difficulties posed by the VFPPS by proposing a new phase-shifting device that operates on the principle of vector summation [4, 5]. The proposed device alleviates the difficulties by eliminating the small optical waveguide loop while maintaining similar performance to the VFPPS, thereby allowing it to operate in the baseband with high cutoff frequencies.

Principle of operation: Fig. 1 shows a block diagram of the proposed broadband phase-shifter using the vector summation method, hence named vector sum phase-shifter (VSPS). The expressions in the square brackets indicate the magnitude and phase of the RF signals at various stages in the VSPS.

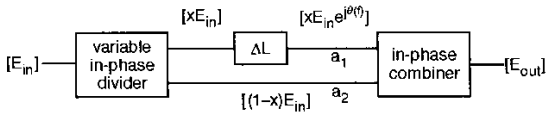

Fig. 1 *Schematic block diagram of broadband VSPS*

From Fig. 1, the transfer function of the VSPS is expressed as

$$H(f) = a_1(1-x) + a_2 x e^{j\theta(f)} \quad (1)$$

where $\theta(f) = -2\pi f n \Delta L/c$ and ΔL is the path length difference between the two arms; n is the refractive index of the delay lines; c is the velocity of light; a_i ($i = 1, 2$) is the individual attenuation (if any) of the arms.

From (1), the minimum phase-shift through the VSPS is zero and the maximum phase-shift through the device is $\theta(f)$. Other phase-shifts in the range between these two values can be obtained by intermediate values of x between 0 and 1. The VSPS therefore behaves like a continuously variable frequency linear phase-shifter.

Like the VFPPS in [3], cancellation of the RF signal from the two distinct paths of the VSPS happens at the device resonant frequencies, which are defined as $f = (m + 0.5)c/(n\Delta L)$ for integer m. Near to these resonant frequencies, the VSPS transfer function exhibits a high loss and poor phase linearity. As such the usable device bandwidth is limited to well below the lowest resonant frequency.

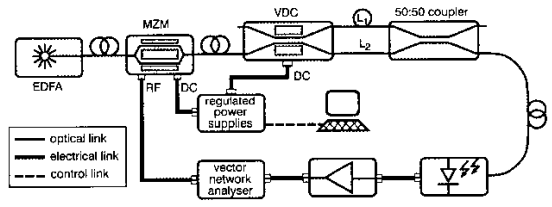

Fig. 2 *Photonic VSPS experiment setup*

Photonic vector sum phase-shifter: To verify the VSPS concept, a photonic implementation of VSPS was prototyped and characterised. The experiment setup is illustrated in Fig. 2.

The photonic implementation of the VSPS is based on the intensity modulation and direct detection technique (IM/DD). Since the VSPS resembles a Mach-Zehnder interferometer, utilising a narrow linewidth